THE JOURNAL OF PHYSICAL CHEMISTRY B

ARTICLE

pubs.acs.org/JPCB

Pattern Formation Kinetics for Charged Molecules on Surfaces: Microscopic Correlation Function Analysis

V. N. Kuzovkov,*[,†,¶] E. A. Kotomin,[‡] and G. Zvejnieks[†]

[†]Institute for Solid State Physics, University of Latvia, Latvia

[‡]Max-Planck Institute for Solid State Research, Stuttgart, Germany

ABSTRACT: The kinetics of pattern formation and phase separation in a system of two types of oppositely charged molecules with competing short- and long-range interactions on surfaces/interfaces is studied combining three methods: a microscopic formalism of the joint correlation functions, reverse Monte Carlo, and nonequilibrium charge-screening factors. The molecular ordering occurs on the background of the Ostwald ripening and thus is strongly nonequilibrium. We have demonstrated how initial random distribution of molecules is changed for loose similar-molecule aggregates, with further reorganization into dense macroscopic domains of oppositely charged molecules. Pattern formation process is characterized by the correlation length which monotonically increases in time.

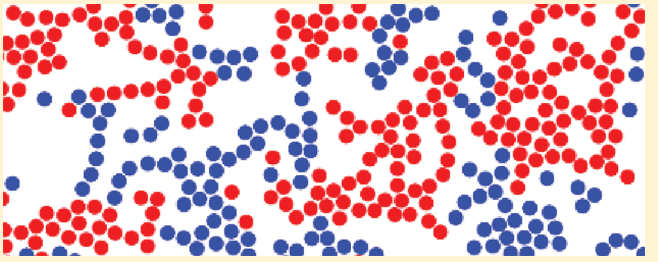

INTRODUCTION

Pattern formation and phase separation in a system of oppositely charged molecules on surfaces/interfaces continues to attract considerable attention due to its fundamental importance and for applications in several areas including polyelectrolytes, biological membranes, etc.[1−5] Most cited theoretical studies are performed at the mesoscopic level where reactant distribution is characterized by concentration fields.[3,6] There is a considerable gap between methods used in the phase separation kinetics (mesoscopic level) and statistics of the equilibrium systems (microscopic level).[7] Note that only the latter approach is able to predict the short and intermediate order in particle (molecule) distribution and characteristic pattern sizes using the very basic information on particle diffusion coefficients and particle interactions.

Most biological systems are mixtures of oppositely charged macroions, which segregate into ionic complexes or complex coacervates.[8] Recently[1] this phase separation has been studied for charged molecules strongly adsorbed on the interface. The mesoscopic linear response theory was used here and combined with molecular dynamics (MD) computer simulations. As a result, lamellar and periodic hexagonal patterns depending on charge stoichiometry were predicted. However, analysis of the time development of these patterns and their stability remains an open question. In fact, even for a weak van der Waals interactions competing with long-range electrostatics, the expected equilibration is difficult to achieve on surfaces during the typical experimental time scale.

Moreover, there is a great need currently in microscopic (atomistic) methods suited to study systems with macroscopic pattern formation; the commonly used molecular dynamics (MD) and kinetic Monte Carlo (kMC) are applicable only to small systems (especially, for charged particles) and also are quite limited in simulation time.

Indeed, systems with pattern formation reveal the correlation lengths ξ increasing with time; as soon as the correlation length (e.g., aggregate size) approaches the linear size of a simulated system, the modeling ends. On the other hand, the time span simulated should match the kinetics of the natural process. In particular, in the above-mentioned case[1] (systems with phase separation) the Ostwald ripening mechanism occurs, when small particle aggregates or molecules are absorbed by larger aggregates. This is a very slow process with nonexponential kinetics (no characteristic relaxation time) where standard MD is not practically applicable. Even in many more simple cases, to obtain a time span of the order of microseconds, several CPU-months to CPU-years are needed. Additional problems arise because long MD simulations are mathematically ill-conditioned: numerical methods produce time-irreversible solutions of the time-reversible dynamical equations.[9] It is not clear which part of the observations of equilibrium comes due to the limited accuracy in the numerical integration of the dynamical equations. Lastly, fundamentally new MD problems arise for chemical reactions in systems with competing long-range and short-range potentials. Strictly speaking, the standard MD method is not applicable here.

The present paper is a continuation of our methodological study in ref 10.

(i) The first part of this paper[10] dealt with applicability of our microscopic approach called many-point densities (of a number of particles)[11,12] for modeling systems with both short- and long-range interactions of molecules. A basic set of coupled integro-differential equations for joint particle

Received: August 9, 2011
Revised: October 3, 2011
Published: November 03, 2011

densities describing relative spatial distributions of molecules, to be solved numerically, is presented and discussed here. In previous studies of systems with Coulomb[13,14] and elastic[15] forces, short-range interactions were neglected.

(ii) The second part of the paper[10] presented a new approach of reverse MC (RMC) that is based on the goodness-of-fit statistical model, e.g., the Pearson χ^2 test for radial distribution functions coming from equations for many-point densities. Use of the RMC is important because the relationship between the calculated radial distribution functions (joint correlation functions) and the molecular distribution in a real space is not obvious and far from trivial. The RMC method is used to visualize the system spatial structure. We discussed in ref 10 only methodological results, such as accuracy of the RMC method (simulation times, convergence of results, additional problems arising for dense ordered structures). The main purpose of the paper[10] was to demonstrate the applicability of the two aforementioned methods, using several typical cases for charged systems.

(iii) Alongside with the many-point densities and RMC, one can use other pattern characterization methods, such as the analysis of the nonequilibrium charge screening. This method was described in our paper in ref 16. As is well-known, particles in equilibrium systems are spatially redistributed in such a way that their effective Coulomb interactions become short-range (Debye−Hückel theory[7]). As we demonstrated in ref 16, this is not the case for kinetics, e.g., for equilibration processes, where we observed such effects as overcharging (charge amplification) and charge inversion. In this paper, we use the ideas of the nonequilibrium charge screening for the analysis of the pattern formation dynamics in systems of charged molecules.

Summing up, in this paper we study the kinetics of pattern formation and phase separation in a system of two types of oppositely charged molecules with competing short- and long-range interactions on surfaces/interfaces combining three methods: a microscopic formalism of the joint correlation functions, reverse Monte Carlo, and nonequilibrium charge-screening factors. The molecular ordering occurs on the background of the Ostwald ripening and thus is strongly nonequilibrium. We demonstrate how initial random distribution of molecules is changed for loose similar-molecule aggregates, with further reorganization into dense macroscopic domains of oppositely charged molecules. This pattern formation process is characterized by the correlation length.

MODEL AND PARAMETERS

Following ref 1, we consider a 2D mixture of oppositely charged molecules A and B with the fixed densities n_A and n_B and diffusion coefficients D_A and D_B. Motions of individual molecules possess a drift in the potential created by all other molecules. Similarly,[1] the pair potentials of the interaction is a sum of the short-range and long-range contributions. The former is the commonly used 6-12 Lennard-Jones (van der Waals) potential ($\nu, \nu' = A, B$)[9]

$$U^{LJ}_{\nu\nu'}(r) = 4U_0\left[\left(\frac{r_0}{r}\right)^{12} - \left(\frac{r_0}{r}\right)^{6} + C_{\nu\nu'}\right] \quad (1)$$

The parameter U_0 is the same for pairs of similar and dissimilar molecules. However, for similar particles $C_{\nu\nu} = 0$, $\nu = A, B$. This choice corresponds to the mutual attraction at distances close to r_0, where r_0 is an effective molecular diameter, and repulsion at short distances. Thus, one takes into account the finite molecule size. For dissimilar molecules AB the potential is shifted, $C_{AB} = 1/4$, and cut at $r_c = 2^{1/6}r_0$.[9] This corresponds to the AB repulsion at distances shorter than r_c.

In its turn, the long-range Coulomb potential reads

$$U^{C}_{\nu\nu'}(r) = \frac{e_\nu e_{\nu'}}{\varepsilon r} \quad (2)$$

where ε is the dielectric constant and e_A and e_B molecule charges. In other words, mobile similar molecules are supposed to show a trend to aggregate which is limited by their repulsion at long distances.

It is convenient to use dimensionless parameters. The spatial scale units could be r_0 whereas time units are $t_0 = r_0^2/D$, where $D = D_A + D_B$ is the coefficient of mutual diffusion. The characteristic temperature based on the Lennard-Jones parameter U_0 is $T_0 = U_0/k_B$, so that one can introduce the dimensionless temperature $\theta = T/T_0$.

The competition between the short-range and long-range potentials is characterized by the parameter $\delta = e^2/\varepsilon r_0 k_B T_0$. The dimensionless density of molecules reads $\eta = nr_0^2$, where $n = n_A + n_B$ and the dimensionless diffusion asymmetry $\mu = D_A/D$. That is, assuming the random molecule distribution, the control parameters are (η, θ, δ, and μ). We consider below the role of these parameters in pattern formation.

The spatial distribution of three types of arbitrary molecular pairs AA, BB, and AB analogously to the radial distribution function in statistical physics of dense gases and liquids[7] is characterized by three joint correlation functions: two for similar particles, $X_\nu(r, t)$, $\nu = A, B$, and a third one for dissimilar particles, $Y(r, t)$, where r is the relative distance between two particles.[11,12] These joint correlation functions are normalized to unity: as $r \rightarrow \infty$, $X_\nu(\infty, t) = Y(\infty, t) = 1$. The deviation of the correlation function above unity means molecule concentration surplus, below unity, depletion with respect to the Poisson distribution. The physical meaning of these correlation functions is the following:[11,12] the quantities

$$C^{(A)}_A(r, t) = n_A X_A(r, t) \quad (3)$$

$$C^{(A)}_B(r, t) = n_B Y(r, t) \quad (4)$$

are average densities of particles A and B, respectively, at the relative distance r provided that a probe particle A is placed into the coordinate origin.

We assume random initial distribution of molecules (taking into account their finite size r_0) which corresponds to a well-stirred system and commonly used in self-organization studies:[11,12] $X_\nu(r, 0) = Y(r, 0) = 0$ for $r \le r_0$, but $X_\nu(r, 0) = Y(r, 0) = 1$ as $r > r_0$. In other words, we consider formation of order from chaos.

Mathematically the problem is reduced to the numerical solution of the set of integro-differential equations with the typical structure[10]

$$\partial g(r, t)/\partial t = r^{-1}\partial[rj(r, t)]/\partial r \quad (5)$$

$$j(r, t) = \partial g(r, t)/\partial r + \partial W[g, r, t]/\partial r g(r, t) \quad (6)$$

dx.doi.org/10.1021/jp207644f | J. Phys. Chem. B 2011, 115, 14626–14633

Here $g(r, t) = X_A(r, t)$, $X_B(r, t)$, and $Y(r, t)$, whereas $W[g, r, t]$ is a nonlinear functional of all three correlation functions (see more detail in ref 10 and in the Appendix).

The calculated time development of the three kinds of the radial distribution functions contains considerable physical information on a two-component system which could be supplemented with the analysis of the Coulombic *screening factors*. Let us assume that the a probe molecule ν = A, B produces at the distance r the *reference* potential $\phi^0_\nu(r) = e_\nu/\varepsilon r$. In a real many-particle system, charges of mobile molecules are spatially rearranged so that the reference potential changes for the effective one, $\phi_\nu(r, t)$. (The relevant equations are presented in ref 10.) In general, the charge screening is nonequilibrium since the effective potential is time-dependent. We studied these charge-screening effects earlier in the kinetics of the diffusion-controlled reactions[13,14] and reconsider here for the case without reaction. For this analysis, we define the two screening parameters $Q_A(r, t)$ and $Q_B(r, t)$: $\phi_\nu(r, t) = Q_\nu(r, t)\phi^0_\nu(r)$, ν = A, B.

The standard Debye−Hückel theory[7] predicts this factor $Q_\nu(r, t)$ to be a time-independent, positive value smaller than unity at short distances and asymptotically striving to zero at long distances. However, this is true only for well-stirred homogeneous systems of charged particles, but as we demonstrate below, it fails in the case of pattern formation. (Detailed study of the nonequilibrium screening physics is discussed in ref 16). Here we used the screening factors as a convenient indicator of the structural changes controlled by a delicate balance of the short-range and long-range forces.

As shown in ref 16, an equilibration process in a closed system with two types of oppositely charged molecules (with short-range interactions inducing a local ordering) does not achieve the Debye−Hückel limit, which is characteristic of steady-state molecule distributions. In all considered cases the structure of the ionic cloud surrounding a probe charged charge is nontrivial and qualitatively different from that expected in the standard Debye−Hückel approach.

The basic assumption of the standard Debye−Hückel theory is a rapid spatial rearrangement of reactants so that each charge A is surrounded by a cloud of oppositely charged particles B which compensates the charge A, and vise versa. However, this simple model turns out to be very limited in the kinetics of diffusion-controlled processes. It is well-known that nonequilibrium effects arise in these systems and for any process where spatial fluctuations are controlled by diffusion. The minimum characteristic lifetime of processes with any spatial fluctuation of particles ν = A, B at the spatial scale ξ can be estimated as $t_\nu = \xi^2/D_\nu$.[11,12] However, when particle interactions are included, the structure formation of the size ξ can take orders of magnitude longer times than the characteristic diffusion time with no correlations. Therefore, at the finite time t the structure at long distances from a probe charge remains nonequilibrium. Furthermore, the transient asymptotics $Q_\nu(\infty, t) = 1$ differs from the (practically nonachievable) equilibrium, $Q_i(\infty, \infty) = 0$.

To visualize the joint correlation functions, we use here the complementary reverse Monte Carlo (RMC) method.[10,17] This allows us to restore structural snapshots at different times t using the calculated radial distribution functions. The RMC technique was proposed for generating particle configurations that are consistent with experimentally measured radial distribution functions or a structure factor. Although at first RMC was designed for liquid and glassy materials,[17] it was later applied to crystalline systems[18] as well. An advantage of the RMC method is based on the fact that no interatomic forces or atomic potentials are necessary. When a randomly selected particle has moved to a new trial position, the new cost function has been recalculated. If the cost function has decreased, this step is accepted; otherwise, the step is rejected in our algorithm (Metropolis algorithm[19]). This method, however, could hardly be used for the ordered, crystalline, and closely packed systems[10] since a structure reconstruction by means of a random particle permutation becomes extremely time-consuming.

RESULTS

Equilibrium and Irreversibility. In forthcoming papers we plan to consider pattern formation in nonequilibrium systems with chemical reactions. Here we restrict ourself with a closed system without reaction characterized by a constant number of molecules. Transient-ordered structures could arise during the equilibration process which is defined by the free energy minimum.[1] In other words, we focus on the kinetics of this process instead of commonly studied thermodynamics. Note that in the system under study similar molecules show a trend to aggregate (under moderate Coulomb interactions). Initial random distribution of molecules is first replaced by a local ordering which leads to a formation of numerous small locally ordered aggregates. At the second stage of the process, these aggregates start to compete and large aggregates grow at the expense of small ones (Ostwald ripening).[20] The small aggregate formation is kinetically favored (they nucleate more easily), whereas growth of large aggregates is thermodynamically driven. The kinetics of this process (which asymptotically could end up with the survival of a single superaggregate) is very slow, and thus only the transient (nonequilibrium) process of the pattern formation during the Ostwald ripening is observed under normal experimental conditions. Thus our study of the equilibration kinetics is complementary to the traditional thermodynamic study.

Standard System. To understand better the pattern formation peculiarities in the two-component system with interplay of the short-range (Lennard-Jones) and long-range (Coulomb) interactions, let us consider first the simplest *standard* system shown in Figure 1 with the Coulomb interactions switched off, $\delta = 0$. In this limiting case the remaining short-range potentials support similar-molecule attraction and dissimilar molecule repulsion. That is, we observe here similar molecule aggregates randomly distributed in space. Note that this structure is not stationary since large aggregates monotonously grow at the expense of small ones. This is a trivial result of the above-discussed Ostwald ripening.[20] For simplicity, we consider here equal molecule mobilities, $D_A = D_B$; $\mu = 0.5$.

The aggregate growth becomes apparent from the joint correlation (radial distribution) functions for similar molecules, $X_A(r, t) = X_B(r, t)$. These functions plotted on the top-left panel in Figure 1 demonstrate a series of peaks corresponding to the formation of the first, second, third, etc. coordination spheres typical for condensed matter. (To make the effect more clear, the logarithmic scale is used.) The formation of the short-range and then intermediate-range order is obviously a non-steady-state process. As it is well observed at relatively low temperatures chosen here, $\theta = 0.35$, the amplitudes of nearest peaks in the radial distribution functions strongly increase in time and tend to become singular. This indicates at the similar-molecule aggregation process, almost regular structure and small dispersion in the relative distances between molecules. It is logical to expect that

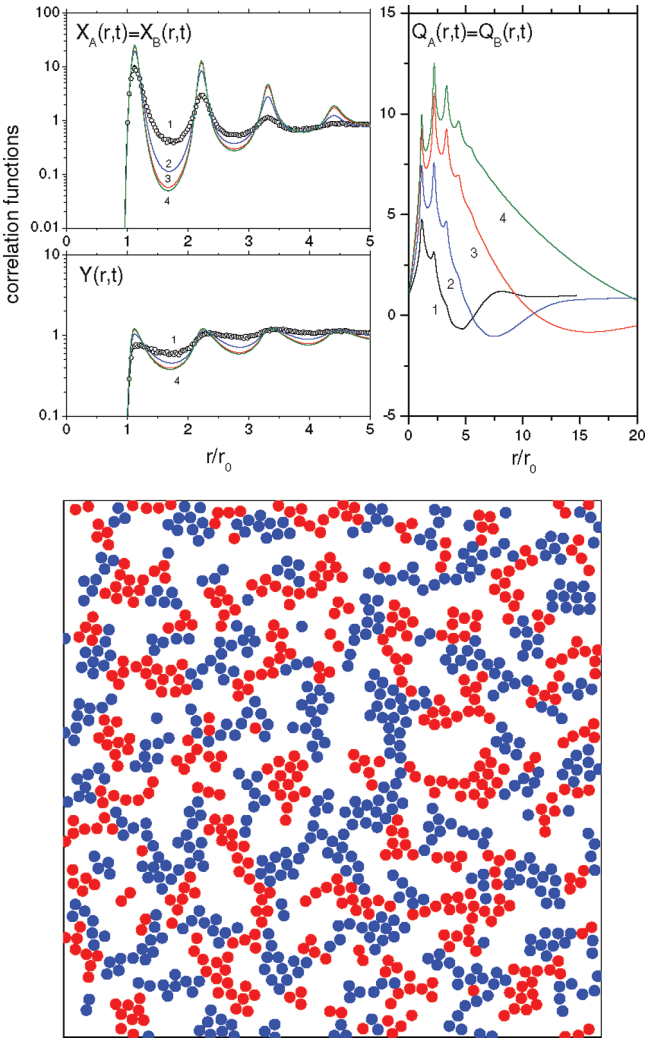

Figure 1. (Color online) Standard system without Coulomb interactions ($\delta = 0$) at low temperature, $\theta = 0.35$. Other parameters: $\eta = 0.4$, $\mu = 0.5$. Dimensionless time: (1) $t = 10^{12}$, (2) $t = 2^{14}$, (3) $t = 2^{16}$, (4) $t = 2^{18}$. In the top-left window are plotted the joint correlation functions $X_A(r, t) = X_B(r, t)$, $Y(r, t)$ [open circles in curves 1 show the correlation functions obtained using the RMC]. The top-right window shows the charge screening parameter $Q_A(r, t) = Q_B(r, t)$. The bottom window shows the typical particle distribution restored using the RMC for case 1.

a local ordering of small aggregates occurs at short distances and leads to systems similar to dense gas or liquid. As soon as aggregates grow, the ordering becomes more and more long-range and could result in formation of microcrystalline structure.

The local ordering for each coordination sphere takes its own characteristic relaxation time. For instance, the curves 3 and 4 in Figure 1 are close; that is, the short-order is already achieved, while for other spheres it takes longer and longer time. A comparison of curve 4 in Figure 1 and curve 1 in Figure 2 for the same (long) time $t = 2^{18}$ but two different temperatures ($\theta =$ 0.35 and $\theta = 0.50$) clearly shows that an increase of the temperature leads to the broadening of the peaks, even in the first and second coordination spheres. This corresponds to a less-ordered system which looks like a dense liquid.

In a wide temporal range, the correlation function for dissimilar molecules $Y(r, t)$ remains close to unity but shows some oscillations. These oscillations correspond to particles A which are located by chance nearby the B aggregate (and vise versa). Since similar molecules in aggregates are locally ordered, this is manifested as an ordering in the surrounding of the probe molecule A, despite the fact that the molecules A in any way referred to this ordering due to neglect of the AB Coulomb interactions.

To visualize the pattern formation, the *snapshot* was obtained using the RMC method (the bottom window in Figure 1 which corresponds to the curve 1 in the correlation functions, the left window). In turn, snapshot coordinates were statistically analyzed, and the corresponding radial distribution function was plotted by open circles in the left window. As one can see, this coincides with the numerical solution of the kinetic equations (a full line). The snapshot clearly demonstrates dissimilar molecule segregation and similar molecule aggregation. At longer times one expects aggregate growth and further similar molecule ordering. However, the RMC fails to reproduce this process.[10]

The flaw of the joint correlation functions used is that these characterize mostly the short-range ordering in the nearest coordination spheres. However, essential fraction of information on the Coulomb interactions is hidden in the correlation function *asymptotics* (small deviations from a standard unity value which hardly could be illustrated graphically). Use of the RMC does not help since charge screening could be achieved even by small molecule movements. This is why sometimes important changes in the system could be unnoticed. However, as we discovered, these are screening factors $Q_A(r, t) = Q_B(r, t)$ which are most sensitive to structure changes. Our approach[10] permits the study of a whole range of the Coulomb interactions. Let us start with the limiting case of very weak Coulomb forces, $\delta \rightarrow 0$. The relevant screening functions are presented in the top-right window in Figure 1. It should be remembered that in the standard Debye–Hückel theory[7] a probe charge is surrounded by a cloud of oppositely charged charges and thus is seen from the outside as the particle with a reduced charge. The Debye–Hückel screening factor is always positive and smaller than unity and asymptotically strives for zero. In our case, however, a probe molecule very likely belongs to the aggregate and thus is surrounded by similar molecules. Thus, it is seen from distances comparable to the aggregate size as the quasi-particle with a large effective charge (e.g., $Q > 10$ in Figure 1). At distances exceeding the average distance between dissimilar aggregates, the screening factor changes its sign since a probe particles now is surrounded with aggregates of *opposite* sign. Note that we discussed earlier the effects of nonequilibrium Coulomb screening in the reaction kinetics between charged particles.[14] It is obvious that the segregation process is not steady state, and aggregate growth is accompanied with the similar growth of the screening parameter maximum which exceeds the value of unity by an order of magnitude.

Note that the correlation functions strongly oscillate, thus reflecting the molecule distribution over nearest coordination spheres. In contrast, the screening factors are relatively smooth; the main attention should be focused not on their fine structure at a spatial scale comparable with r_0 but more on a scale characterized by a global increase/decrease and change of sign. Note that we consider here processes in condensed matter rather than plasma. The charges (electrons) in plasma are very mobile and rapidly equilibrate; in contrast, in our case molecular diffusion is quite slow, and thus molecule distribution is usually far from equilibrium. Thus, the screening factors become strongly time-dependent. In our case the short-range Lennard-Jones

dx.doi.org/10.1021/jp207644f |J. Phys. Chem. B 2011, 115, 14626–14633

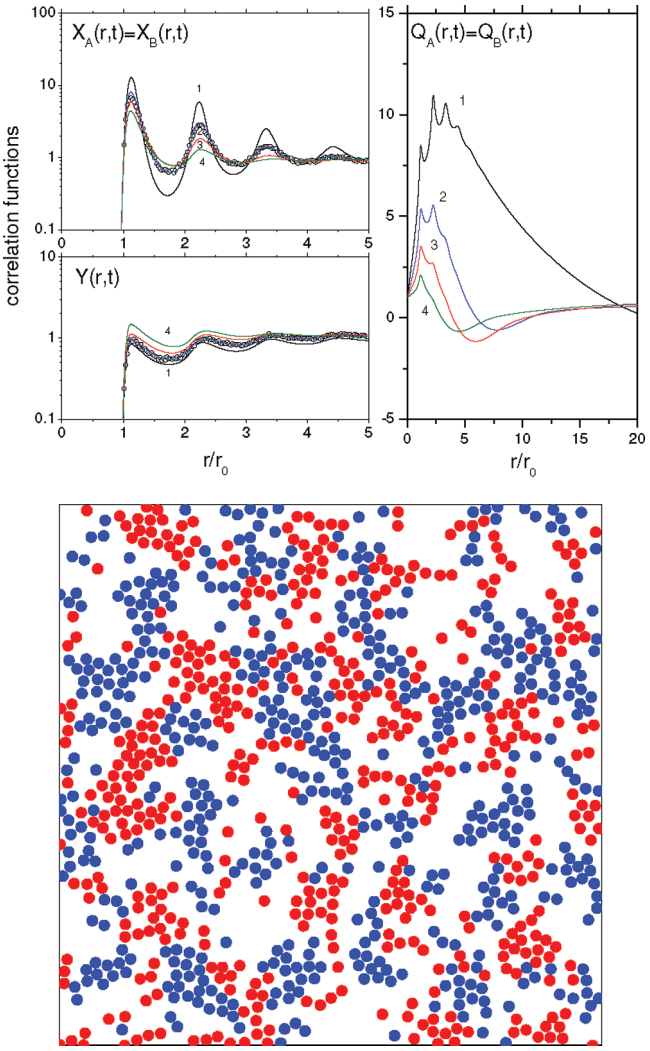

Figure 2. (Color online) Effect of weak Coulomb interactions at relatively high temperatures $\theta = 0.5$ for a fixed time $t = 2^{18}$. Parameters are $\eta = 0.4, \mu = 0.5$. The Coulomb interactions are: curve 1, $\delta = 0$; curve 2, $\delta = 0.05$; curve 3, $\delta = 0.1$; curve 4, $\delta = 0.2$. The similar and dissimilar correlation functions $X_A(r, t) = X_B(r, t)$, $Y(r, t)$ are presented in the top-left window. The correlation functions calculated using the RMC are shown by open circles in curves 2. The top-right window shows the charge-screening factors $Q_A(r, t) = Q_B(r, t)$. The bottom window shows the fraction of a snapshot obtained for curve 2 using RMC.

potential plays also an important role; in the above-considered limiting case of $\delta = 0$, the nonequilibrium structure was created only due to short-range interactions. We discuss below how this structure is changed when the Coulomb interaction is taken into account.

Despite the fact that an analysis of the Coulomb screening in the limiting case of infinitely weak interactions, $\delta = 0$, looks purely formal, it demonstrates the *instability* mechanism which makes the system of charged molecules structurally different from the above-considered standard system. The difference is that despite the fact that charged aggregates could exist, their unlimited growth is impossible due to increasing mutual molecule repulsion. What is important is that the mutual attraction of similar-charge aggregates becomes possible, if these aggegates are separated by aggregates with the opposite charges. This is a reason for the possible formation of the lamellar structure consisting of alternating A- and B-type dense domains, to be discussed below.

Weak Coulomb Interaction. Let us consider now the same system of oppositely charged molecules with a finite but small Coulomb interaction, $\delta \leq 0.2$, shown in Figure 2. A comparison of the radial distribution functions is performed here for a fixed time $t = 2^{18}$ but different interaction energies ($\delta = 0$ [curve 1] corresponds to the *standard* system discussed above). As compared to Figure 1, the temperature here is increased, $\theta = 0.5$.

The analysis of the correlation functions for similar and dissimilar molecules shows that the distributions are not steady-state since the aggregates did not reach yet the optimal size. Moreover, we did not even reach the stage of the real interaction between aggregates of dissimilar types. This is seen from a scale of amplitudes in oscillations of the correlation function of dissimilar molecules $Y(r, t)$ which are an order of magnitude smaller that those for similar molecules. (This is also true for the standard system, Figure 1). In other words, the observed small oscillations in the $Y(r, t)$ distribution arise from a random interaction of molecules A with aggregates B (and vise versa), but molecules ordering inside A-, B-aggregates practically is independent of a weak dissimilar AB aggregate interactions.

The Coulomb interaction makes aggregates more loose and smaller in size. This could be concluded from analysis of the screening factors: increase of δ leads to the decrease of Q peak maximum and the characteristic distance at which Q changes its sign. The snapshot in Figure 2 is similar to that in Figure 1. In both cases A aggregates are surrounded by B aggregates. However, this is not real pattern formation, but rather a more or less random distribution of aggregates with dissimilar molecules as a result of the segregation process. Therefore, once more the Ostwald ripening is observed here. An additional effect of the *dissimilar* molecule aggregation via Coulomb interactions, happening within considered time scale is discussed below. Note that the Ostwald ripening exists only under certain conditions, as demonstrated in Figure 3. At high temperatures aggregation could be strongly limited even by a relatively weak Coulomb interaction, $\delta = 0.20$. The curves 1−4 in this figure practically coincide which means that the steady state is established in the first coordination spheres (short-range order). In other words, simple structures appear as typical for dense gases and liquids. Additional information could be obtained from the screening factors: their time dependence indicates gradual structural rearrangements at long distances. The snapshot shows clearly that the system is close to a well-stirred two-component liquid rather similar-molecule aggregates as discussed above.

Domain and Lamellar Structure Formation. Based on the above-presented results, the conclusion could be drawn that compact aggregates could be created at relatively low temperatures, Figure 4. Even more so, the similar-molecule aggregates exist even for strong Coulomb interactions (we consider here $\delta = 0.40$). A comparison of the screening parameters with and without Coulomb interactions, Figure 1, shows considerable structural changes. Now the maximum Q does not exceed the value of 2 (instead of 10−12 without Coulomb interactions) which indicates that the aggregates are smaller and more compact. The oscillations in the screening factors increase in time (e.g., curve 4) which indicates the formation of closely packed domain structures, similar to those considered earlier in macroscopic analysis.[1] This is a modification of the Ostwald ripening process. In previous cases only similar molecule aggregates were observed; here two-component aggregates appear where dissimilar molecules are also ordered.

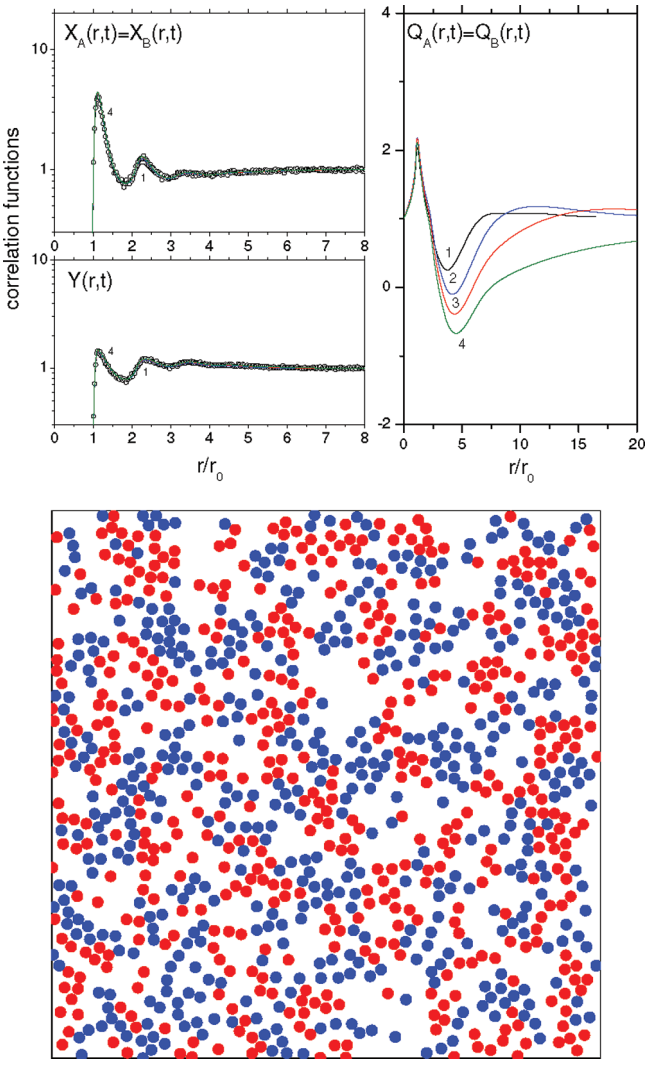

Figure 3. (Color online) Similar to Figure 1 for moderate Coulomb interaction, $\delta = 0.20$, at high temperature, $\theta = 0.50$. Other parameters: $\eta = 0.4$, $\mu = 0.5$, time: curve 1, $t = 10^{12}$; curve 2, $t = 2^{14}$; curve 3, $t = 2^{16}$; curve 4, $t = 2^{18}$. The circles in curves 4 show the correlation functions obtained using RMC; the snapshot in the bottom window corresponds to the distribution function 4.

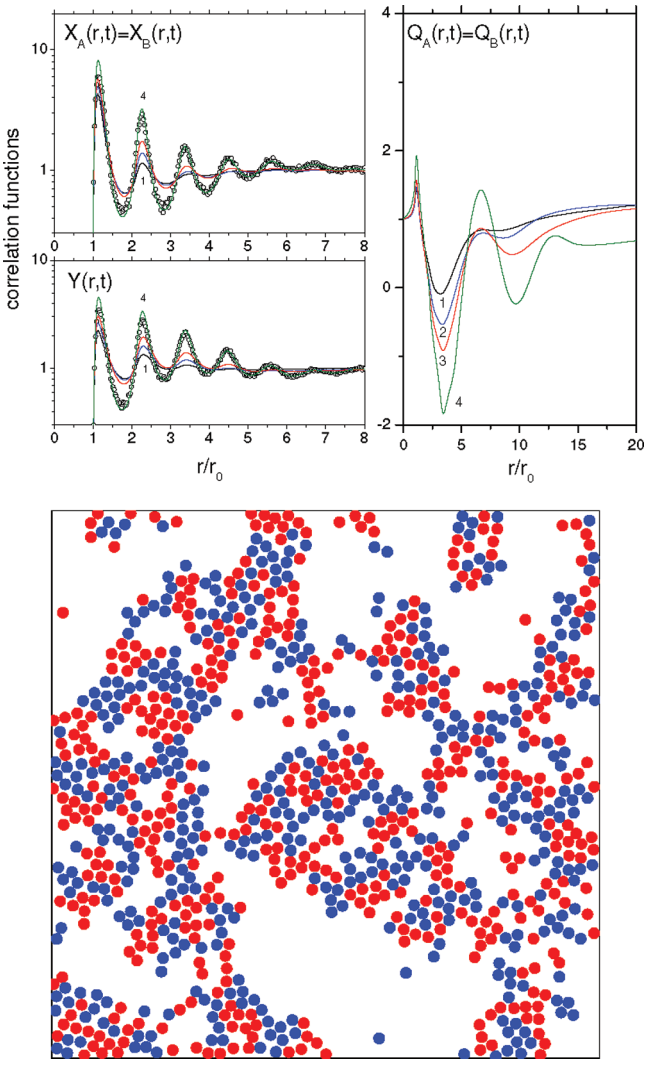

Figure 4. (Color online) As in Figure 1 for a strong Coulomb interaction, $\delta = 0.40$, at low temperatures, $\theta = 0.35$. Other parameters: $\eta = 0.4$,$\mu = 0.5$; time: curve 1, $t = 10^{12}$; curve 2, $t = 2^{14}$; curve 3, $t = 2^{16}$; curve 4, $t = 2^{18}$.

The disoriented domain structure formation is confirmed by the snapshot in Figure 4. This structure is energetically favorable due to the remote attraction of similar aggregates (say, A) via attraction of each of A to dissimilar aggregates B between them. The observation of a locally ordered AB molecular structure (rather than a random mixture of dissimilar aggregates) is confirmed by the correlation function of dissimilar molecules $Y(r, t)$. The amplitude of its oscillations is now comparable with that for the similar molecules, which was not observed in all previous cases, Figure 1 and Figure 2.

The temporal evolution of this system is obvious: first of all, AB domain structure slowly transforms into lamellar one; second, large domains will continue their continuous growth at the expense of small domains. The non-steady-state nature of this process is confirmed by the screening parameters in Figure 4 which continuously change with time.

Asymmetry in Mobilities and Charges. To check the role of asymmetry in molecules A and B mobilities and charges, as well as the role of system density, additional calculations were performed. The analysis of the screening parameters Q_A, Q_B for the case of $D_B/D_A = 1/9$ (Figure 5) shows their similarity. Highly mobile molecules at a given time t establish the intermediate order at the larger distances as compared to less mobile molecules; that is, A, B molecular structures differ by the relaxation times.

Another important parameter is the system dimensionless density, η. As follows from Figure 6, this parameter also determines mainly the relaxation time; the system density here is decreased twice as compared to previous cases (Figures 1−5). The screening factor in Figure 6a (plotted as a function of the Coulomb interaction δ) shows at the same time $t = 2^{18}$ the same trend as for larger density (Figure 2), but with smaller aggregates (see peak amplitudes for the screening factors). Respectively, at shorter times the aggregates does not have enough time to be formed (Figure 6b). Therefore, the asymmetry in mobilities μ and density η are basically the *kinetic* parameters determining the time scale (relaxation time) of processes.

We modeled also the asymmetry in molecule charges as discussed also in ref 1. It was assumed that $Z_B/Z_A = 3$, due to

dx.doi.org/10.1021/jp207644f |J. Phys. Chem. B 2011, 115, 14626–14633

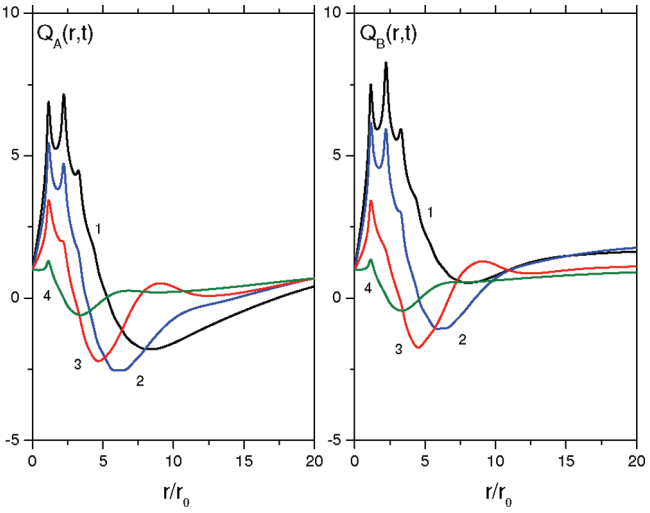

Figure 5. (Color online) Screening factors, $Q_A(r, t)$ and $Q_B(r, t)$, for asymmetric diffusion, $D_B/D_A = 1/9$. Coulomb interactions: curve 1, δ = 0.05; curve 2, δ = 0.10; curve 3, δ = 0.20; curve 4, δ = 0.40. Other parameters: $\eta = 0.4$, $\theta = 0.4$, time $t = 2^{18}$.

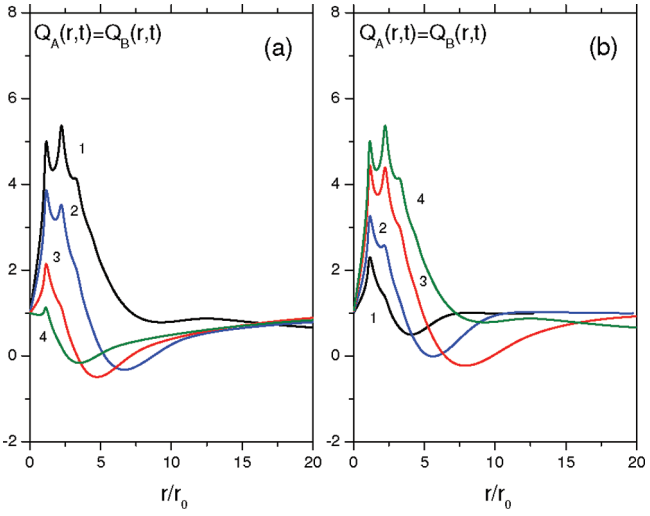

Figure 6. (Color online) As in Figure 5 for a low density, $\eta = 0.2$, and intermediate temperature $\theta = 0.4$. (a) Coulomb interactions: curve 1, δ = 0.05; curve 2, δ = 0.10; curve 3, δ = 0.20; curve 4, δ = 0.40. Time $t = 2^{18}$. (b) Coulomb interaction $\delta = 0.05$. Time: (1) $t = 10^{12}$, (2) $t = 2^{14}$, (3) $t = 2^{16}$, (4) $t = 2^{18}$.

system electroneutrality and molecule densities, $n_A/n_B = 3$. The analysis of the screening factors for systems with larger density but smaller charges suggests that the chosen Coulomb interaction $\delta = 0.3$ is relatively small for molecules A but large for B's.

In fact, no steady state is observed in Figure 7, as the size of A aggregates continuously increases. Since the chosen value of δ is too large for B's, *no* aggregates of this type could be created. This is why $Q_B(r, t)$ reveals no peak (typical for aggregatization), but instead it sharply decreases at short distances. The A aggregates are attracted as earlier at the distances larger than the aggregate size, and the same is true also for B molecules. As a result, one can expect formation at long times of large domains A dissolved by (preferentially single) molecules B which keeps the electroneutrality

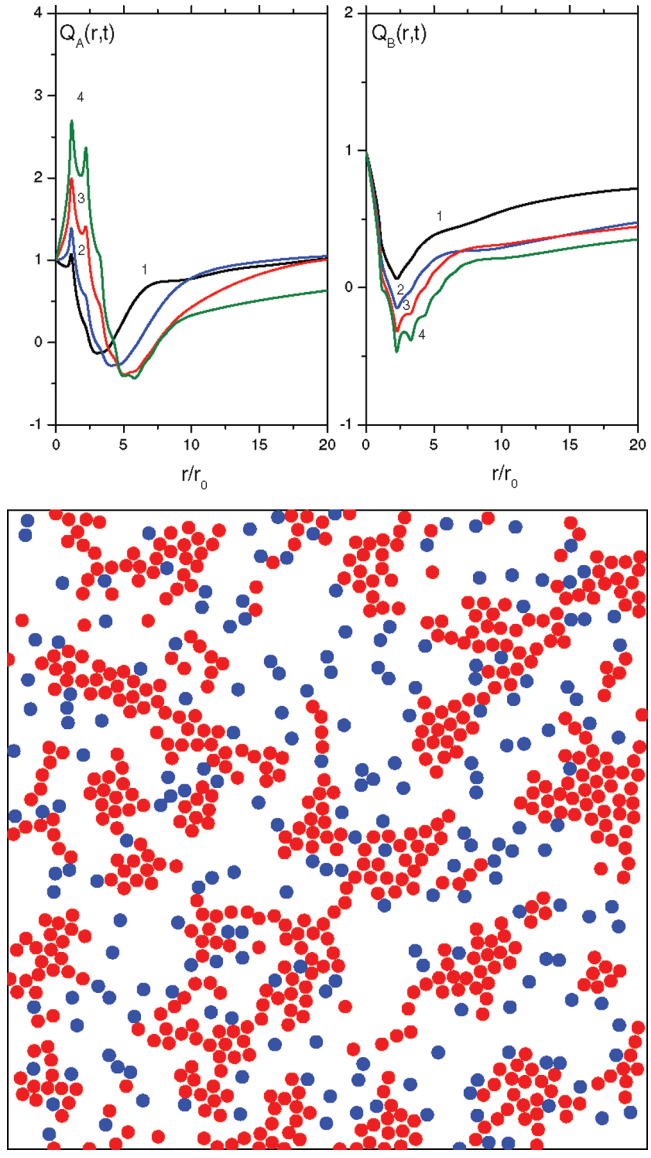

Figure 7. (Color online) Screening factors, $Q_A(r, t)$ and $Q_B(r, t)$, for asymmetrical charges, $Z_A = 1$ and $Z_B = 3$. Other parameters: $\theta = 0.40$, $\delta = 0.30$, $\eta = 0.32$, $\mu = 0.5$. Time: (1) $t = 10^{12}$, (2) $t = 2^{14}$, (3) $t = 2^{16}$, (4) $t = 2^{18}$. The snapshot to the right-hand side is obtained for the distribution function 4.

of the whole system. The size of B aggregates could be probably increased reducing the Coulomb interaction δ.

CONCLUSIONS

The present microscopic analysis based on the joint correlation functions of the 2D system consisting of oppositely charged molecules at surfaces/interfaces clearly demonstrated that the formation of mesoscopic domain (lamellar) patterns could occur for relatively strong Coulomb interactions and low temperatures. The temperature and the ratio of the Coulomb and short-range parameters are the two *control* parameters, whereas system density and ratio of diffusion coefficients are the *kinetic* parameters. In a given range of parameters, the structure rapidly relaxes to the quasi-equilibrium. Such a structure with short-range ordering is similar to dense gas/liquid. However, our main

dx.doi.org/10.1021/jp207644f |J. Phys. Chem. B 2011, 115, 14626–14633

interest is focused on the cases with the Ostwald ripening. Under these conditions the system is considerably nonequilibrium, which leads to various kinds of pattern formation. Their building elements are molecular aggregates (both homogeneous and heterogeneous) with further growths of large aggregates at the expense of small ones. We have also demonstrated here that most of earlier observed structures (e.g., in MD modeling) in fact are nonequilibrium with respect to the continuous growth of molecular aggregates. A comparison of these results with predictions for the reversible chemical reactions is of great interest.

APPENDIX

Detailed analysis of our method is presented in ref 10. The process kinetics is described by the following set of integro-differential equations for the correlation functions of similar, $X_\nu(r, t)$, and dissimilar, $Y(r, t)$, molecules:

$$\partial Y(r,t)/\partial t = \nabla \mathbf{j}(r,t) \tag{7}$$

$$\mathbf{j}(r,t) = D\left(\nabla Y(r,t) + \frac{Y(r,t)}{k_B T}\nabla W_{AB}(r,t)\right) \tag{8}$$

$$\partial X_\nu(r,t)/\partial t = \nabla \mathbf{j}_\nu(r,t) \tag{9}$$

$$\mathbf{j}_\nu(r,t) = 2D_\nu\left(\nabla X_\nu(r,t) + \frac{X_\nu(r,t)}{k_B T}\nabla W_{\nu\nu}(r,t)\right) \tag{10}$$

Here $W_{\nu\nu'}(r, t)$ are the effective interaction energies and D_ν are mutual diffusion coefficients, $D = D_A + D_B$. These equations describe the time development of the closed system of interacting molecules A, B toward the equilibrium. The main problem here is that the effective interaction energies W, in turn, are complicated integral functionals of the correlation functions sought for. Even more so, these functionals reveal singularities at short relative distances (molecule repulsion) and oscillate at the distances corresponding to the emerging aggregates. That is, this is a nontrivial computational problem.

For the illustration, we demonstrate here the two examples of the functionals to be solved numerically. In the Coulombic system the potential of a particle in the coordinate origin reads[10,14]

$$\phi_A(r,t) = \frac{e_A}{\varepsilon r} + \frac{e_A n_A}{\varepsilon}\int \frac{[X_A(r',t) - Y(r',t)]\mathrm{d}x'\mathrm{d}y'}{|\mathbf{r} - \mathbf{r}'|} \tag{11}$$

Despite that this result is based on the Debye−Hückel approach,[7] no system equilibrium is assumed here.

More complicated nonlinear functionals arise due to the short-range (Lennard-Jones) potentials, and we obtain the differential relations as follows:

$$\nabla W^{LJ}_{AA}(r,t) = \nabla U^{LJ}_{AA}(r) + n_A\int \nabla U^{LJ}_{AA}(r'')X_A(r'',t)X_A(r',t)\,\mathrm{d}\mathbf{r}' + n_B\int \nabla U^{LJ}_{AB}(r'')Y(r'',t)Y(r',t)\,\mathrm{d}\mathbf{r}' \tag{12}$$

Equations 12 are derived in the Kirkwood superposition approximation for three-point particle densities[21] (see also ref 22). We discussed similar functionals in our methodological papers[11,12] but so far never performed practical calculations. The main reason was that in the systems with oscillating correlation functions (our case of the Lennard-Jones potentials) the difference equations with small coordinate increments $\Delta r \ll r_0$ should be used. Taking into account that the functionals themselves are integral relations, their numerical calculations needed a decade ago[11,12] enormous computational time. However, these calculations became possible nowadays.

AUTHOR INFORMATION

Corresponding Author

*E-mail: kuzovkov@latnet.lv.

Present Addresses

[¶]Northwestern University, Evanston, United States.

ACKNOWLEDGMENT

This work was supported by ESF grant 2009/0202/1DP/1.1.1.2.0/09/APIA/VIAA/141 (G.Z.). Authors are greatly indebted to M. Olvera de la Cruz for numerous fruitful discussions.

REFERENCES

(1) Loverde, S. M.; Solis, F. J.; Olvera de la Cruz, M. *Phys. Rev. Lett.* **2007**, *98*, 237802.

(2) Kung, W.; Solis, F.; Olvera de la Cruz, M. *J. Chem. Phys.* **2009**, *130*, 044502.

(3) De Decker, Y.; Marbach, H.; Hinz, M.; Guenther, S.; Kiskinova, M.; Mikhailov, A. S.; Imbihl, R. *Phys. Rev. Lett.* **2004**, *92*, 198305.

(4) Hsiao, P.-Y.; Luijten, E. *Phys. Rev. Lett.* **2006**, *97*, 148301.

(5) Tretiakov, K. V.; Bishop, K. J. M.; Kowalczyk, B.; Jaiswal, A.; Poggi, M. A.; Grzybowski, B. A. *J. Phys. Chem. A* **2009**, *113*, 3799–3803.

(6) Okuzono, T.; Ohta, T. *Phys. Rev. E* **2003**, *67*, 056211.

(7) Balescu, R. *Equilibrium and Non-equilibrium Statistical Mechanics*; Wiley: New York, 1975.

(8) Raspaud, E.; Olvera de la Cruz, M.; Sikorav, J.-L.; Livolant, F. *Biophys. J.* **1998**, *74*, 381–393. Kalsin, A. M.; Fialkowski, M.; Paszewski, M.; Smoukov, S. K.; Bishop, K. J. M.; Grzybowski, B. A. *Science* **2006**, *312*, 420–424.

(9) Frenkel, D.; Smit, B. *Understanding Molecular Simulation*; Academic Press: New York, 2001.

(10) Kuzovkov, V. N.; Kotomin, E. A.; Zvejnieks, G.; Olvera de la Cruz, M. *Phys. Rev. E* **2010**, *82*, 021602.

(11) Kotomin, E. A.; Kuzovkov, V. N. *Rep. Prog. Phys.* **1992**, *55*, 2079–2188.

(12) Kotomin, E. A.; Kuzovkov, V. N. *Modern Aspects of Diffusion-Controlled Reactions: Cooperative Phenomena in Bimolecular Processes*; Comprehensive Chemical Kinetics Vol. 34; Elsevier: North Holland, Amsterdam, 1996.

(13) Kuzovkov, V. N.; Kotomin, E. A. *Chem. Phys.* **1985**, *98*, 351–360.

(14) Kuzovkov, V. N.; Kotomin, E. A.; von Niessen, W. *J. Chem. Phys.* **1996**, *105*, 9486–9492. Kuzovkov, V. N.; Kotomin, E. A.; von Niessen, W. *Phys. Rev. E* **1996**, *54*, 6128–6138.

(15) Kuzovkov, V.; Kotomin, E. *J. Chem. Phys.* **1993**, *98*, 9107–9114. Kuzovkov, V. N.; Kotomin, E. A.; von Niessen, W. *Phys. Rev. B* **1998**, *58*, 8454–8463.

(16) Kuzovkov, V. N.; Kotomin, E. A.; Olvera de la Cruz, M. *J. Chem. Phys.* **2011**, *135*, 034702.

(17) McGreevy, R. L.; Pusztai, L. *Mol. Simul.* **1988**, *1*, 359–367. McGreevy, R. L. *Nucl. Instrum. Methods Phys. Res., Sect. A* **1995**, *354*, 1–16. McGreevy, R. L. *J. Phys.: Condens. Matter* **2001**, *13*, R877–R913.

(18) Tucker, M. G.; Dove, M. T.; Keen, D. A. *J. Appl. Crystallogr.* **2001**, *34*, 630–638.

(19) Metropolis, N.; Rosenbluth, A. W.; Rosenbluth, M. N.; Teller, A. H.; Teller, E. *J. Chem. Phys.* **1953**, *21*, 1087–1092.

(20) Boistelle, R.; Astier, J. P. *J. Cryst. Growth* **1988**, *90*, 14–30.

(21) Kirkwood, J. G. *J. Chem. Phys.* **1935**, *76*, 479–493.

(22) (a) Mai, J.; Kuzovkov, V. N.; von Niessen, W. *Physica A* **1994**, *203*, 298–315. (b) Mai, J.; Kuzovkov, V. N.; von Niessen, W. *J. Chem. Phys.* **1994**, *100*, 6073–6081.